Int J Adv Manuf Technol (2016) 84:2649–2657
DOI 10.1007/s00170-015-7917-1

ORIGINAL ARTICLE

Three-dimensional laser drilling of polymethyl methacrylate (PMMA) scaffold used for bone regeneration

Keyvan Rahmani-Monfard[1] · **Alireza Fathi**[1] · **Sayed Mahmood Rabiee**[1]

Received: 17 April 2013 / Accepted: 28 September 2015 / Published online: 5 October 2015

Abstract Development of new methods of scaffold fabrication that closely mimic the structure and function of the extracellular matrix (ECM) is one of the main issues in tissue engineering. This study aims to present a newly developed predefined three-dimensional polymethyl methacrylate (PMMA) scaffold fabricated via CO_2 laser drilling technique. To achieve this goal, using a computer-controlled laser drilling machine, arrays of interconnected holes with a predefined pattern and geometry were drilled on bulk PMMA samples. Three groups of scaffolds with increasing levels of porosity, and pore sizes of 490±10 μm, were fabricated and evaluated for compressive properties. In order to promote their bioactivity, a thin layer of chitosan/β-TCP composite was coated on the surface of the fabricated samples. Morphology of bulk PMMA scaffolds and PMMA scaffolds with chitosan/β-TCP composite coating were studied using scanning electron microscopy (SEM). Moreover, cell viability was assessed by SaOS-2 cells. Results indicate that this technique allows the fabrication of scaffolds with high amount of interconnectivity and controllability of porosity, pore size, and mechanical properties, the advantage that other methods lack. Furthermore, chitosan/β-TCP composite coating improves the interaction between osteoblast-like cells and the polymeric scaffolds and accelerates the rate of cell proliferation.

Keywords Scaffold · Bone tissue · PMMA · Laser drilling · Composite

✉ Alireza Fathi
fathi@nit.ac.ir

[1] Department of Mechanical Engineering, Babol University of Technology, Babol, P. O. Box 484, Iran

1 Introduction

Design and fabrication of porous scaffolds is a crucial field of study in tissue engineering. Three-dimensional (3D) tissue scaffold plays a vital role in cell attachment, proliferation, and new tissue formation. Scaffolds as artificial extracellular matrices are able to drive and support three-dimensional tissue regeneration.

Autografts, in fact, are strictly limited by the volume of bone that can be safely obtained and by donor site morbidity. On the other hand, allografts induce the possibility of immune rejections or disease transfers [1–3]. An ideal scaffold for tissue-engineering applications should have special characteristics in order to function as a true substitute that satisfies the patient-specific biological, mechanical, and geometrical requirements. Such characteristics can be summarized as the following: (1) a network of interconnected pores so that cells can migrate, differentiate, and attach deep within the scaffolds; (2) channels which provide paths for oxygen and nutrients to cells deep inside the scaffold and for the waste products to be easily carried away; (3) biocompatibility and bioactivity with a high affinity for cells to attach and proliferate; (4) proper shape; and (5) appropriate mechanical strength that matches the surrounding bone properties [4–7].

Most of the available scaffold fabrication methods such as solvent casting, fiber bonding, phase separation, gas-induced foaming, and salt leaching are either limited to producing scaffolds with simple geometry or depend on the indirect casting method for scaffold fabrication [8–10]. These methods result in structures of random internal architecture and have great variations from part to part. Solid free-form fabrication (SFF) techniques, also known as additive manufacturing (AM) or rapid prototyping (RP) methods, have attracted lots of attention in recent years. These methods enable design and fabrication of anatomically shaped scaffolds with varying

internal architectures using virtual 3D computer models. They allow precise control over porosity, pore size, permeability, and stiffness. Control over these characteristics may give rise to cell infiltration and mass transport of nutrients and metabolic waste throughout the scaffold [11–13]. The three main categories of AM systems are as follows: powder-based systems (e.g., selective laser melting (SLM) and three-dimensional printing (3DP)), solid-based systems (e.g., fused deposition modeling (FDM) and laminated object manufacturing (LOM)), and liquid-based systems (e.g., stereolithography (SLA), Polyjet 3D Printing and Thermal Phase Change Inkjet) [14]. In spite of their advantages, on the negative side, there are still some limitations in using SFF methods. The materials which are available for RP use will depend on the process chosen and are still relatively limited. In SLA system, the photopolymers are expensive and perishable and working with liquid materials can be messy and the fabricated parts require a post-curing operation in a separate oven-like apparatus for complete cure and stability. In SLS system, it takes a considerable cool-down time before the part can be removed from the machine. Large parts with thin sections may require as much as two days of cooling. In FDM method, the finished parts are anisotropic, that is, they exhibit different mechanical characteristics in different directions. 3DP systems are limited to the resolution, surface finish, part fragility, and available materials. All thermal phase change inkjets have material limitations and make fragile parts. In some indirect SFF methods, the fabricated parts experience dimensional changes or may inherit errors and defects from the molding process such as cracks [15–20]. Development of laser processing, including surface patterning, surface modification, and drilling has taken a considerable interest in medical science. Laser processing makes it possible to machine very small holes and allows precise control over the size of drilled holes. Moreover, it is a non-contact technique and can be used on a vast variety of materials [21–24].

As far as the laser source is concerned, most biomaterials especially polymers show a high amount of power absorption of CO_2 laser with wavelength of 10.6 μm, Excimer laser with wavelength of about 190–248 nm, and third harmonic of solid-state laser of 355 nm [25]. Polymers due to some of their unique characteristics are used widely in the field of tissue engineering. Poly methyl methacrylate (PMMA) is a polymer that has been successfully utilized as a bone filler and bone substitute due to its remarkable biocompatibility, processability, and low cost [26, 27]. Moreover, PMMA fits well in the field of laser machining since the removal mechanism is generated by vaporization and the vapor products are volatile monomers (MMA) [25]. Notwithstanding PMMA is bioinert, non-degradable, and hydrophobic, thus, bone-like apatite cannot be readily formed on the surface of this polymer [28]. Coating a biologically active material like chitosan/β-TCP composite is one clear solution for promoting the capability of bone regeneration of PMMA. In tissue engineering applications, chitosan has been described as a delivery system able to carry active agents and growth factor [29, 30]. Chitosan has a wide variety of applications in the biomedical fields such as bone reconstruction, cell encapsulation, and drug delivery [31, 32]. However, its bioactivity needs to be boosted by adding bioactive materials such as calcium phosphates [33]. β-Tricalcium phosphate (β-Ca3 (PO4) 2=β-TCP) is one of the most important calcium phosphates with excellent biocompatibility and osteoconductivity properties [34].

The objective of the present study is to develop a novel method of producing a predefined 3D porous PMMA scaffold appropriate for bone regeneration by using the CO_2 laser drilling technique. To achieve this goal, based on a predefined pattern, a framework of interconnected holes was drilled on bulk PMMA. Afterwards, a thin layer of chitosan/β-TCP composite was coated on the scaffold so as to enhance the bioactivity and the proliferation of osteoblast-like cells. We will show that the proposed technique provides some advantages such as enhanced control over the scaffold porosity and its pore architecture, including size, orientation, branching, and interconnectivity. Unlike the available fabrication methods, the proposed method of this study ensures high level of interconnectivity of porous structure because the channel pattern is defined in a way that channels intersect with each other. High level of interconnectivity leads to adequate delivery of cells and nutrient supply during subsequent culture throughout the complete porous scaffold, and therefore, osteoblasts migration, adhesion, proliferation, and differentiation inside the pores would be induced [35]. Three-dimensional and connective network configuration could enhance osteogenesis, and it is expected to provide paths for efficient bone ingrowth. Direct bone formation may also be affected by pore geometry. Furthermore, chitosan/β-TCP composite film can provide favorable conditions for the biological functions of PMMA.

2 Materials and methods

2.1 Experimental setup and procedure

The experimental setup for the laser drilling process is shown in Fig. 1. The experiments were conducted using a 100-W carbon dioxide (CO_2) laser (Fanavaran Laser Sahand Company, Iran). The spot diameter of the laser beam was 300 μm. The laser system was integrated with a two-axis CNC table which is directed to move across the entire machining area and a shutter that controls the laser on/off state. Argon with a 3.2-bar pressure was used as a shield gas.

In the earlier investigation, authors developed a model by applying two neuro-fuzzy systems to predict the geometrical characteristics of the drilled holes. To achieve this goal, first,

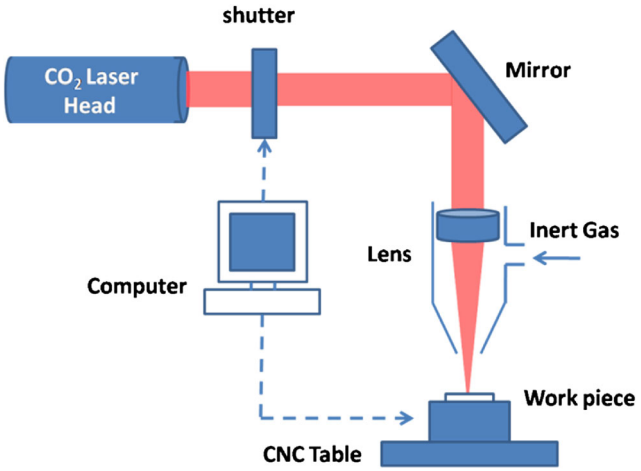

Fig. 1 The laser drilling setup showing the PMMA work piece on the *X-Y* plane of the CNC table with the laser focused along the *Z* axis to the work piece

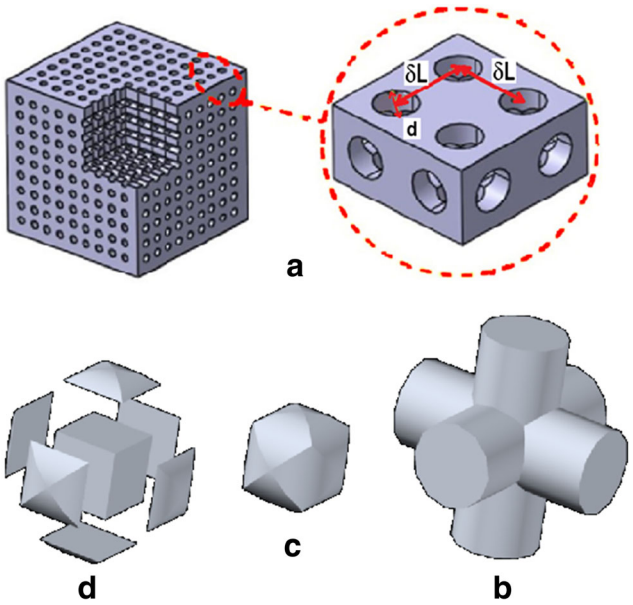

Fig. 2 The schematic model of the 3D scaffold (**a**) showing orthogonal and interconnected repeating array of through holes making a porous network structure; **b** three orthogonal intersecting holes; **c** the intersecting volume; **d** decomposing the intersecting volume into a cubic and six remaining parts

some experiments were conducted to investigate the influence of laser power and laser irradiation time on the holes entrance diameters, hole exit diameters, and depth of drilled holes. Then, based on the results, experimental models of the process were developed [36]. The model was used to calculate values of laser power and laser irradiation time that lead to desirable hole dimensions including depth and diameter. In order to obtain a 3D porous scaffold, first, cubic bulk PMMA samples with length of 10 mm were prepared and then repeating arrays of open-ended holes were drilled on three sides of bulk samples. Consequently, an orthogonal and highly interconnected channel network was produced. The center distance (δL) of channels was controlled by the movement of the CNC table.

2.2 Porosity

Porosity refers to the percentage fraction of voids in the entire scaffold volume. Three parameters, namely the depth of drilled hole (H), hole diameter (d), and center distance (δL), are used to calculate the amount of porosity (Fig. 2a). Since in this study, the fabricated scaffold has a regular network, the scaffold porosity can be estimated precisely by calculating the amount of removed material and its initial volume. Assuming a fully interconnected network, the porosity of a cubic scaffold is calculated as follows:

$$V_{\text{bulk}} = L^3 \tag{1}$$

$$V_{\text{removed}} = 3N^2AH - 2N^3 * V_{\text{intersect}} \tag{2}$$

$$N = \frac{L}{\delta L} \tag{3}$$

$$H = \min(H, L) \tag{4}$$

$$Porosity = \frac{V_{\text{removed}}}{V_{\text{bulk}}} * 100 \tag{5}$$

where L is the cubic length, N is number of holes in each dimension, A is the hole cross section area, H is the hole length, and $V_{\text{intersect}}$ is the intersection volume of three intersecting orthogonal holes (Fig. 2b–d). This intersecting volume can be computed using the following relation [37]:

$$V_{\text{intersect}} = 2d^3 \int_0^{\pi/4} \int_0^1 s\sqrt{1-s^2\cos^2 t}\, ds\, dt = \left(2-\sqrt{2}\right)d^3 \tag{6}$$

In order to specify the accuracy of this formula, the porosity of the samples was also calculated by measuring their dimension and weight according to the following equation [38]:

$$\text{Porosity } (\%) = 1 - \frac{\rho_{\text{scaffold}}}{\rho_{\text{material}}} \tag{7}$$

where ρ_{scaffold} is the apparent density of porous PMMA measured by dividing the weight by the volume of the samples and ρ_{material} is the density of the material of which the scaffold is fabricated.

2.3 Compressive strength

The compression strength of bulk PMMA and PMMA scaffolds was determined using a Universal mechanical tester (Universal, SANTAM, Iran) with a 25-KN load cell. The specimens were bulk cubic shape with 10 mm length. The speed of the Universal tester crosshead was set at 5 mm/min and according to ASTM D695 standard the load was applied until a 30 % reduction in specimen height was achieved. Five samples were tested to obtain the average value.

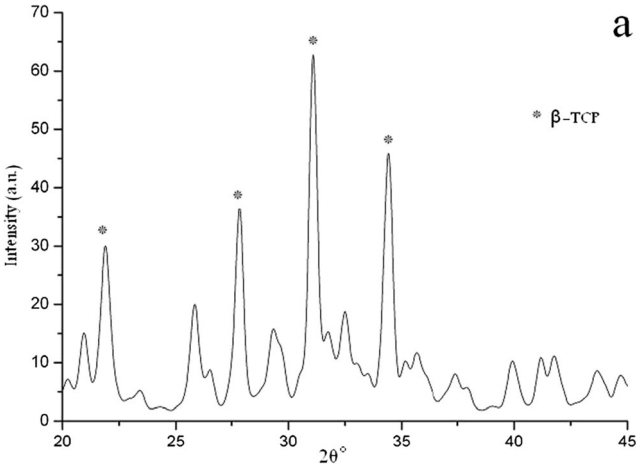

Fig. 3 XRD patterns of synthesized powder produced by sol–gel process. The peaks indicate that the single phase of β-TCP was successfully synthesized

2.4 Preparation of chitosan/β-tricalcium phosphate composite

In this research, analytical grade (Merck, Germany) phosphate pentoxide (P_2O_5) and calcium nitrate tetrohydrate ($Ca(NO_3)_2.4H_2O$) are selected for synthesizing β-tricalcium phosphate (β-TCP, $Ca_3(PO_4)_2$, Ca/P=1.5) powders. In the sol–gel process, at first a specific amount of P_2O_5 and $Ca(NO_3)_2.4H_2O$ was dissolved in absolute ethanol with 10.5 pH. The mixture of solutions was continuously stirred about 30 min at room temperature, then it was heated in a water bath at 60 °C for 1 h, and finally, a white transparent gel was obtained. The gel was dried at 80 °C for 24 h in an air oven and then it was calcined in a furnace at 700 °C for 3 h. The calcined powders were sintered for 2 h at 1200 °C, and then they were placed in air to cool down to ambient temperature. Finally, the sintered products were crushed into the resultant granule using an agate mortar. Powder X-ray diffraction (XRD) patterns were recorded using a Philips PW 1371 diffractometer with Cu $K\alpha$ radiation. The XRD patterns of the synthesis powder are presented in Fig. 3. The pattern for sample shows well-characterized peaks of pure β-TCP, and the peaks were indexed according to the standard pattern (JCPDS 09-0169). These results indicate that single phase of β-TCP was successfully synthesized by sol–gel method.

Chitosan solution of 2 % wt. was prepared by dissolving chitosan in 1 % (*v*/*v*) acetic acid aqueous solvent at 55 °C. Then, NaOH particles were added to the resultant solution to reach PH 7.0. In order to obtain a β-TCP solution of 3 % wt., β-TCP particles were added drop by drop to the chitosan solution, while the solution was being agitated. Then, the chitosan–TCP dispersion was vigorously mixed using a magnetic stirrer for 12 h to obtain a homogenous mixture. At the next stage of the process, the prepared PMMA scaffolds were dipped into the composite solution and rotated for 2 min to form a uniform coating. The coated scaffolds were dried for 48 h and were kept for further tests.

2.5 Cell proliferation rate on the scaffold

In order to examine whether the chitosan/β-TCP composite films prepared in this study exert cytotoxic effects on SaOS-2 cells, we performed proliferation assay. The osteoblast-like cells were extracted from adult rabbit back shank. The cells were washed twice with phosphate buffer solution (PBS), and then they were collected via centrifugation. In the standard incubation condition (5 % CO_2, 37 °C), the cells were incubated for about 1 week in different culture media containing Dulbeco's modified Eagle's medium (DMEM), dexamethasone, vitamin C, and β-sodium glycerol-phosphate. The ostoeblast-like cells were further incubated in DMEM solution at 1×10^4 cells/ml for cell cultivation. The cells were supplemented with 10 % FBS for 7 days in the standard culture condition. In characterization of cell attachment, the samples were taken out for digestion with 0.25 % trypsin EDTA solution. Afterwards, the number of cells was evaluated by hemacytometer.

3 Results and discussion

In the present study, three-dimensional laser drilling of PMMA scaffold used for bone regeneration was investigated. Three sets of samples with increasing levels of porosity were fabricated. The laser parameters and their values are shown in Table 1. These conditions lead to forming holes with the diameter range of 490±10 μm and depth of 12 mm. Figure 4a, b

Table. 1 The table indicates process parameters and the resulted porosity and strength for three groups of scaffolds

Sample series	Laser power (W)	Laser irradiation time (ms)	Center distance (mm)	Predicted porosity (%)	Actual porosity (%)	Compressive strength (Mpa)
1	26	500	1	44.26	43±3	52±7
2	22	500	0.875	55.08	53±1	28±2
3	22	500	0.75	70.01	61±3	20±2

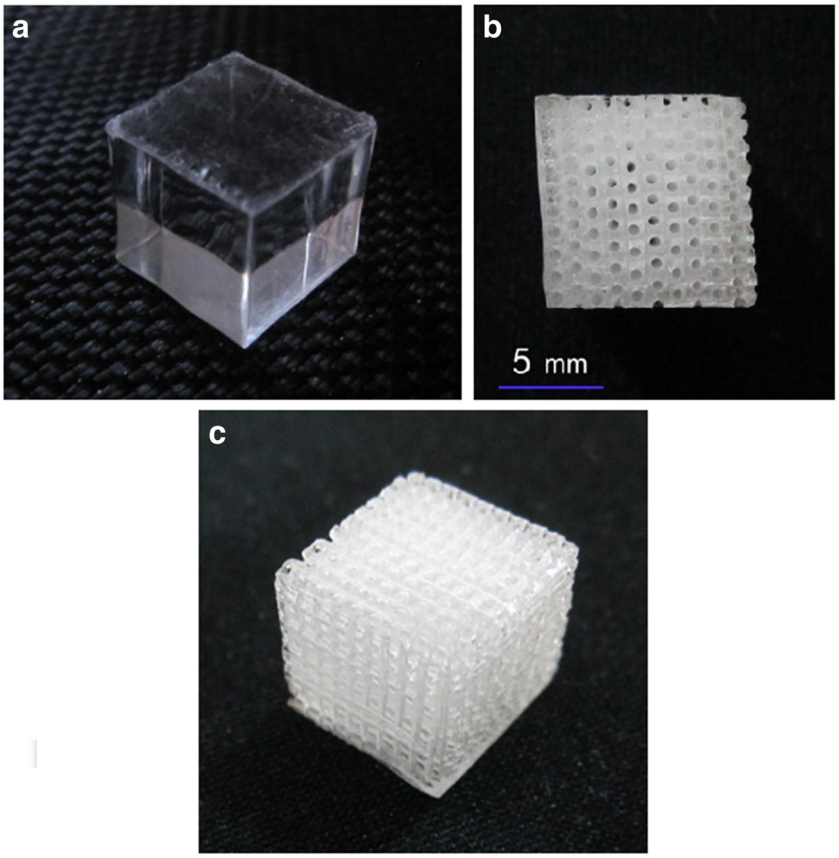

Fig. 4 **a** Bulk cubic specimen before laser processing. **b** A front view of the fabricated PMMA scaffold showing regular pattern of holes made by laser processing. **c** An isometric view of the scaffold showing the 3D network of holes

indicates specimens before and after laser processing, respectively. As can be seen, a regular 3D network of holes has been formed. All the channels are the same size and the center distance between two adjacent channels in each row is equal.

The actual and the predicted amounts of porosity for scaffolds are reported in Fig. 5. Channel size and center distance are the two factors that control the amount of porosity. A large center distance will result in a less porous scaffold while a low

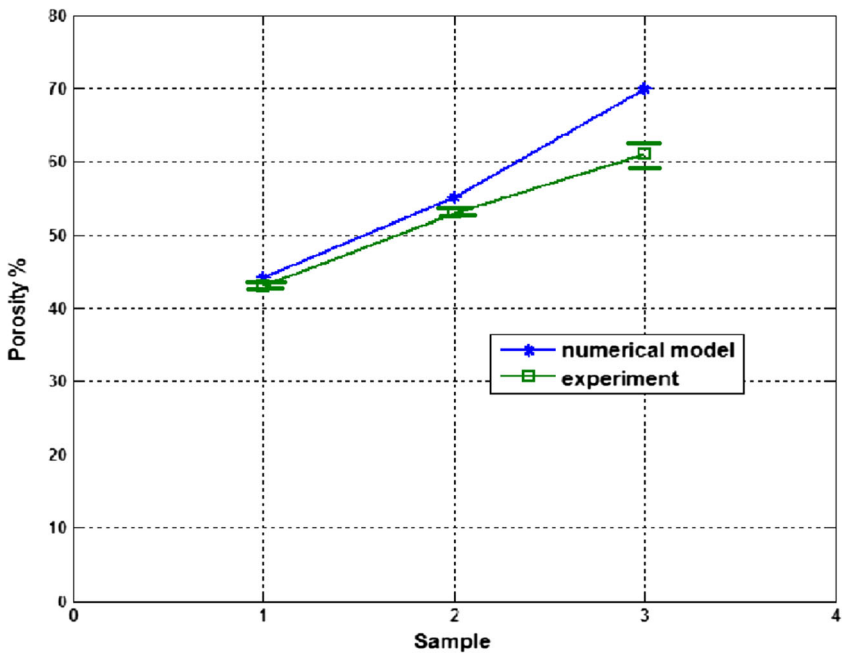

Fig 5 The figure shows the difference in the amount of measured porosity and predicted porosity. A correlation coefficient of 0.854 exists between predicted porosity and actual porosity of scaffolds

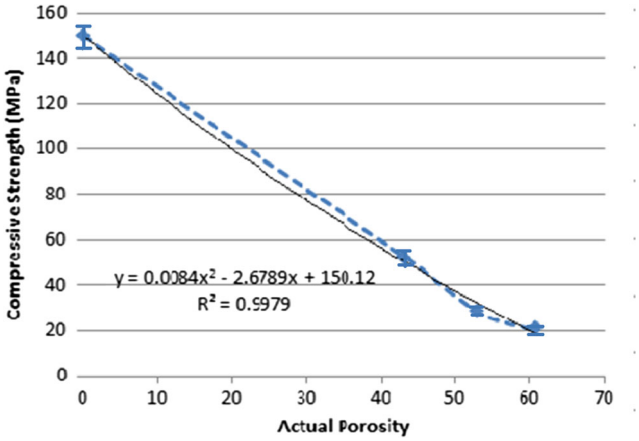

Fig 6 The effect of porosity on compressive strength illustrates a remarkable decrease in compressive strength from 150 to 20 (Mpa) when the porosity increases from 43 to 60 %

center distance will produce a highly porous scaffold. The hole diameters have a similar behavior with some more complexity. The reported values lead to produce scaffolds with actual porosity of 43±3, 53±, and 60±3 % and predicted porosity of 44.26, 55.08, and 70.01 %. According to the results, a correlation coefficient of 0.854 exists between predicted porosity and actual porosity of scaffolds. This close correlation will enable fabrication of specific porosity by compensating for the fact that the amount of actual scaffold porosity is 2–10 % lower than the predicted porosity. One of the major advantages of our method is reproducibility that other traditional methods of fabricating scaffold may lack.

The scaffolds have to possess sufficient strength and stiffness similar to the surrounding bone repair sites that will bear in vivo loads. In order to determine the effect of porosity on mechanical properties, five specimens from each set were used for compressive testing and the average values were obtained.

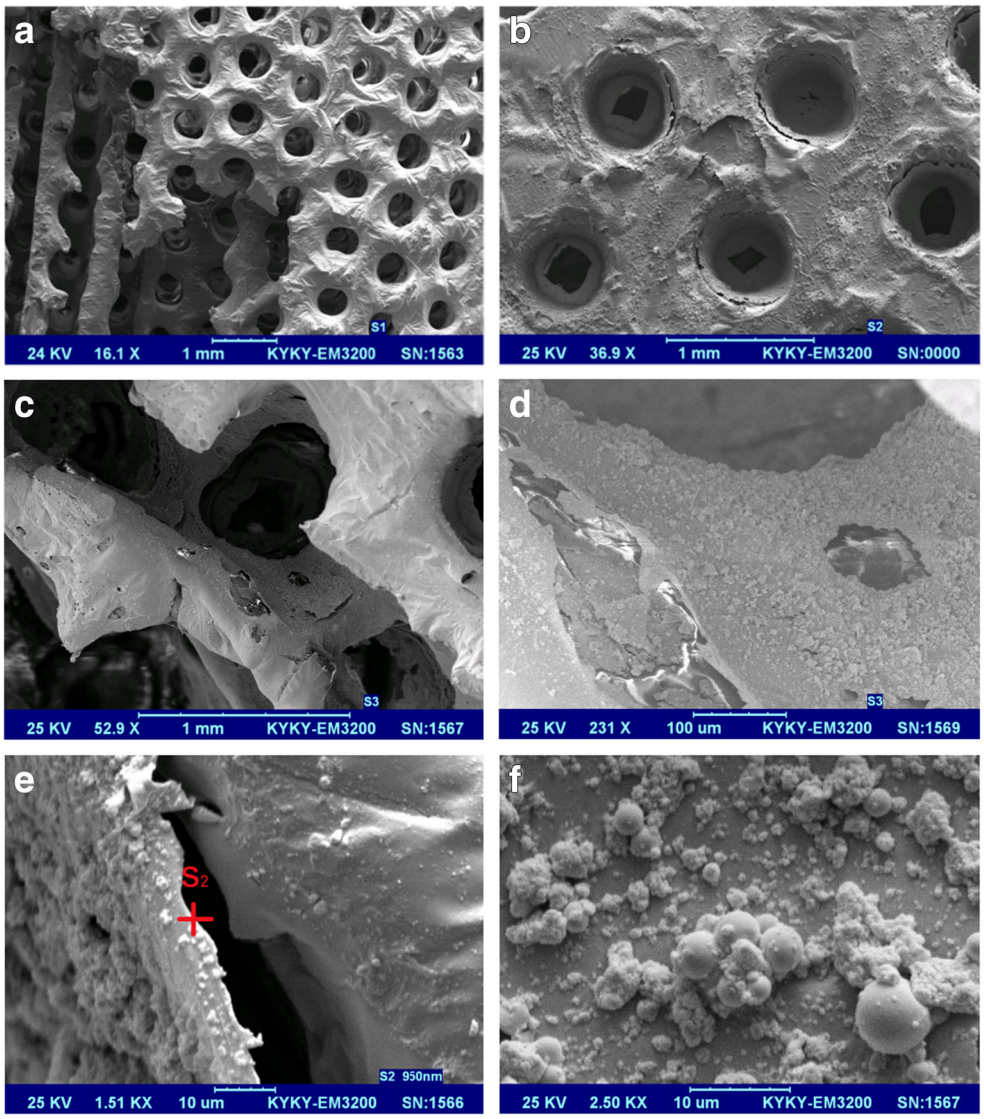

Fig. 7 **a** SEM micrographs of broken part of a scaffold without coating illustrating connective network configuration and open pore structure, **b** a scaffold coated with chitosan/β- TCP composite, and respective magnifications showing details of **c**, **d** the inner surface morphology coated with composite film showing the success in coating of the inner surfaces by immersing the samples in the composite solution (**e**) the thickness of the coated layer and (**f**) distribution of TCP particles

Table 1 shows the compression strength of the fabricated samples with different porosities. These results show that porosity greatly affects the compressive strength of porous PMMA and the less porous scaffolds had better overall properties. On the other hand, laser drilling is often associated with undesirable thermal effects called heat-affected zone (HAZ) leading to surface micro-cracking. Although mechanical properties are mainly affected by the amount of porosity, the authors believe by controlling the laser parameters, a thinner HAZ, and as a result better mechanical properties can be achieved. Investigation about the effects of laser parameters on thickness of HAZ is beyond the scope of this paper. The predicted porosity for each scaffold was plotted via compression strength for the purpose of relating compressive mechanical properties to porosity (Fig. 6). As it can be seen, the compressive strength decreased remarkably from 150 to 20 MPa as the porosity increased from 43 to 60 %. Based on the obtained experimental data, the following experimental model is identified.

$$S = 0.008\mathrm{Por}^2 - 2.678\mathrm{Por} + 150.1 \quad (8)$$

$$R^2 = 0.997 \quad (9)$$

where S is mechanical strength (Mpa) and Por is the scaffold porosity (%).

Figure 7a indicates the SEM image of the broken part of the scaffold. As it can be seen, the scaffold possesses regular and highly interconnected channel structure. The channels are straight and drilled through the entire height of the scaffold. Figure 7b indicates that the channels are cylindrical with the diameter range of 590±10 μm, which is appropriate for bone ingrowth. Based on previous studies, the minimum channel size is supposed to be ≈100 μm because of cell size, migration requirements, and transport [39]. However, channel size bigger than 300 μm is proposed, due to enhanced new bone formation. In bone tissue engineering, to ensure a rapid tissue penetration, a scaffold with relatively large channels (0.5–1 mm) is preferred because the large pores lead to direct osteogenesis [7]. Figure 7c illustrates a rough surface with irregularities that have been formed after laser processing. During drilling, bulges can form on the inside walls of the hole and the surface of the specimen adjacent to the hole edge. We believe that bulge formation plays a positive role in improving surface properties of the scaffolds. In general, all biomedical implants undergo some kind of surface modification before clinical insertation. Most surface modifications of implants employ techniques that increase the roughness of the surface resulting in surface irregularities. Increasing implant surface roughness may allow for an increase in surface area contact as well as an increase in the depth of the interdigitation and mechanical interlocking effect [40–43]. A rough surface is an ideal texture as it usually extends the range of bone-bonding and fosters attachment of progenitor cells, proteins, and bone proliferation cells. In addition, it fosters absorption of biological metabolites [43].

In order to promote the capability of bone regeneration of PMMA, a chitosan/TCP composite was prepared and coated on the inner and the outer scaffold surface by immersing the samples into the composite solution. It is difficult to form calcium phosphate film on PMMA due to the hydrophobicity of the PMMA surface [28]. Chitosan takes the role of a binder and leads to a better adhesion of TCP particles on the scaffold surface. On the other hand, chitosan enhances the bioactivity of PMMA and can be degraded by enzymes in the human body environment and the resulting degradation products are non-toxic [44]. The high magnification SEM micrograph indicates the composite layer formed within the scaffold matrices as well as scaffold outer surface (Fig. 7c, d). A rough layer with a thickness of 950 nm has covered the surface (Fig. 7e). Rough texture which covers the scaffold surface is a key factor to foster the attachment of bone proliferation cells [45]. Images reveal that in some areas, pores are occupied with the composite fully or partially. Although some of the pores are filled, the composite layer degrades gradually after implantation and bone growth will occur. It is worthwhile to mention that PMMA cannot be degraded by body enzymes and as a result, it remains in the body and supports the generated three-dimensional tissue. It is possible to note some white spherical agglomerates on the surface, which can be identified as the β-TCP particles (Fig. 7f).

As a tissue engineering scaffold, a key property of the biomaterial used is its interaction with the target cells. Cell

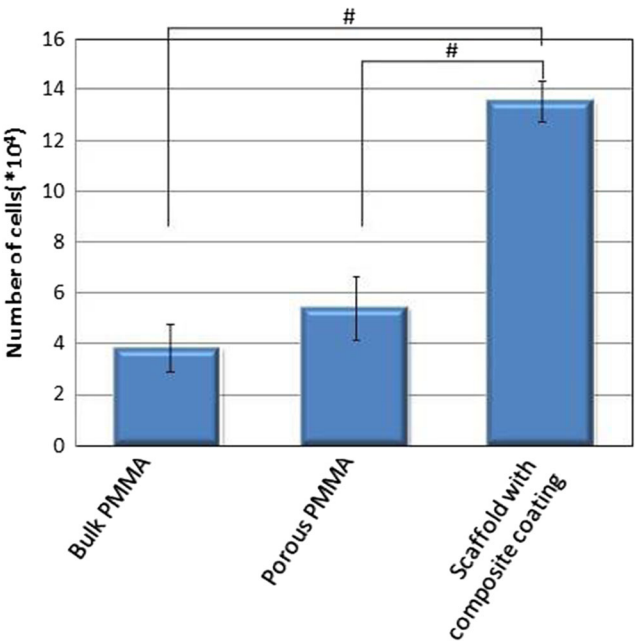

Fig. 8 Proliferation rate of SaOS-2 cells cultivated on the scaffolds. Cells were seeded on the scaffolds with or without chitosan/ β-TCP composite coating for 7 days. The amount of cells is expressed as mean±SD (n=4). #Significant difference between bulk and coated PMMA scaffolds and likewise porous and coated PMMA scaffolds within the same culture condition and time point (P<0.05)

behavior would be different in responding to surfaces with different chemical conditions. In the present study, we have investigated the proliferative behavior of osteoblast-like cells on three surfaces: bulk PMMA, porous PMMA, and PMMA with chitosan/β-tricalcium phosphate composite coating. Achieving this goal, SaOS-2 cells were seeded on the scaffolds. Figure 8 represents the cell proliferation rate of osteoblast-like cells on the surface of various samples after 1 week of cell cultivation. There was a statistically significant difference in the cell numbers over the cultivation time. It was found that PMMA scaffolds with chitosan/β-tricalcium phosphate composite coating were more suitable for osteoblast like cells adhesion and proliferation in comparison with the bulk and porous PMMA scaffolds indicating that chitosan/β-TCP composite film prepared in the current study were cytocompatible.

4 Conclusion

This research presents a laser drilling technique that was successfully developed to produce a 3D porous PMMA scaffold with a highly interconnected porous structure and reproducible porosity, pore size, and mechanical properties. In addition, this study demonstrated that cell compatibility of PMMA scaffolds is greatly enhanced with chitosan/β-TCP composite coating. Osteoblast-like cell attachment and bioactivity on the chitosan/β-TCP composite coating were found to be more significant compared to the findings with the bulk and porous PMMA. Therefore, The PMMA scaffold coated with chitosan/β-TCP layer is recommended to be highly beneficial in bone tissue engineering applications.

References

1. I. Asahina, I. Seto, M. Oda, E. Marukawa, A.M. Imranul, S. Enomoto, Bone Engineering, 1st edition, Em squared, Toronto, 1999.
2. Goulet JA, Senunas LE, DeSilva GL, Greenfeild ML (1989) Autogenous iliac crest bone graft complications and functional assessment. Clin Orthop Relat Res 339:76–81
3. Younger EM, Chapman MW (1989) Morbidity at bone graft donor sites. J OrthopTrauma 3:192–195
4. Fang Z, Starly B, Sun W (2005) Computer-aided characterization for effective mechanical properties of porous tissue scaffolds. Computer-Aided Design 37:65–72
5. Liu C, Xia Z, Czernuszka J (2007) Design and development of three-dimensional scaffolds for tissue engineering. Chem Eng Res Des 85:1051–1064
6. An SH, Matsumoto T, Miyajima H, Nakahira A, Kim KH, Imazato S (2012) Porous zirconia/hydroxyapatite scaffolds for bone reconstruction. Dent Mater 28:1221–1231
7. Liu YL, Schoenaers J, de Groot K, De Wijn JR, Schepers E (2000) Bone healing in porous implants: a histological and histometrical comparative study on sheep. Mater Sci Mater Med 11:711–717
8. Sun W, Darling A, Starly B, Nam J (2004) Computer-aided tissue engineering: overview, scope and challenges. Biotechnol Appl Biochem 39:29–47
9. Sun W, Starly B, Darling A, Gomez C (2004) Application to biomimetic modeling and design of tissue scaffolds. Computer-aided tissue engineering, Biotechnol Appl Biochem 39:49–58
10. Rabiee SM, Moztarzadeh F, Kenari HS, Solati-Hashjin M (2007) Preparation and properties of a porous calcium phosphate bone graft substitute. Materials Sci-Poland 25:1019–1028
11. Fu Q, Saiz E, Rahaman MN, Tomsia AP (2011) Bioactive glass scaffolds for bone tissue engineering: state of the art and future perspectives. Mater Sci Eng C 31:1245–1256
12. Duan B, Wang M (2010) Encapsulation and release of biomolecules from CaeP/PHBV nanocomposite microspheres and three-dimensional scaffolds fabricated by selective laser sintering. Polym Degrad Stab 95:1655–1664
13. Simpson RL, Wiria FE, Amis AA, Chua CK, Leong KF, Hansen UN, Chandrasekaran M, Lee MW (2008) Development of a 95/5 poly(L-lactide-co-glycolide)/hydroxylapatite & beta-tricalcium phosphate Scaffold as bone replacement material via selective laser sintering. Biomed Mater Res-Part B: Appl Biomater 84:17–25
14. Kruth JP, Leu MC, Nakagawa T (1998) Progress in additive manufacturing and rapid prototyping. CIRP Ann Manuf Technol 47(2):525–540
15. Jijotiya D, Verma PL (2013) A survey of performance based advanced rapid prototyping techniques. Sch J Eng Tech 1(1):4–12
16. Gideon NL, Ralf S, Kruthb JP (2003) Rapid manufacturing and rapid tooling with layer manufacturing (LM) technologies, state of the art and future perspectives. CIRP Ann Manuf Technol 52:589–609
17. Mahindru DV, Mahendru P (2013) Review of rapid prototyping-technology for the future. Computer Sci Technol Graphics & Vision 13:27–38
18. Osama AM, Abdelaal, Saied MH, Darwish (2013) Review of rapid prototyping techniques for tissue engineering scaffolds fabrication. Advanced Struct Mater 29:33–54
19. Landers R, Pfister A, Hubner U, John H, Schmelzeisen R, Mulhaupt R (2002) Fabrication of soft tissue engineering scaffolds by means of rapid prototyping techniques. J Mater Sci 37(15): 3107–16
20. Hutmacher WD, Sittinger M, Risbud MV (2004) Scaffold-based tissue engineering: rationale for computer-aided design and solid free-form fabrication systems. Trends Biotechnol 22:354–362
21. Pfleging W, Bruns M, Welle A, Wilson S (2007) Laser-assisted modification of polystyrene surfaces for cell culture applications. Appl Surf Sci 253:9177–9184
22. Aguilara CA, Lua Y, Maob S, Chena S (2005) Direct micropatterning of biodegradable polymers using ultraviolet and femtosecond lasers. Biomaterials 26:7642–7649
23. Rosen JM, Grosser M, Hentz VR (1990) Preliminary experiments in nerve regeneration through laser-drilled holes in silicon chips. Restor Neurol Neurosci 2:89–102
24. Man HC, Wang Q, Guo X (2010) Laser surface microdrilling of Ti and laser gas nitrided Ti for enhancing fixation of dental implants. Opt Lasers Eng 48:583–588
25. Romoli L, Tantussi G, Dini G (2011) Experimental approach to the laser machining of PMMA substrates for the fabrication of microfluidic devices. Opt Lasers Eng 49:419–427
26. Han J, Ma G, Nie J (2011) A facile fabrication of porous PMMA as a potential bone substitute. Mater Sci Eng C 31:1278–1284
27. Boger A, Bohner M, Heini P, Schwieger K, Schneider E (2008) Performance of vertebral cancellous bone augmented with compliant PMMA under dynamic loads. Acta Biomater 4:1688–1693

28. Choi S-M, Yang W-K, Yoo Y-W, Lee W-K (2010) Effect of surface modification on the in vitro calcium phosphate growth on the surface of poly(methyl methacrylate) and bioactivity. Colloids Surf B Biointerfaces 76:326–333
29. Denkbas EB, Ottenbrite RM (2006) Chitosan drug delivery systems: based on their geometries. Bioact Comp Polym 21:351–368
30. Nie HN, Lee LY, Tong H, Wang CH (2008) PLGA/chitosan composites from a combi- nation of spray drying and supercritical fluid foaming techniques: new carriers for DNA delivery. Controlled Release 129:207–214
31. Wang J, Fu W, Zhang D, Yu X, Li J, Wan C (2010) Evaluation of novel alginate dialdehyde cross-linked chitosan/calcium polyphosphate composite scaffolds for meniscus tissue engineering. Carbohydr Polym 79:705–710
32. Muzzarelli R. AA (2009) Chitins and chitosans for the repair of wounded skin, nerve, cartilage and bone. Carbohydr Polym 76: 167–182
33. Tai HY, Fu E, Don TM (2012) Calcium phosphates synthesized by reverse emulsion method for the preparation of chitosan composite membranes. Carbohydr Polym 88:904–911
34. Rabiee SM, Moztarzadeh F, Solati-Hashjin M, Salimi-Kenari H (2008) Porous tricalcium phosphate as a bone substitute. Am Ceramic Soc Bull 87:43–45
35. Hutmacher DW (2000) Scaffolds in tissue engineering bone and cartilage. Biomaterials 21:2529–2543
36. Rahmani-Monfared K, Fathi A, Mozaffari A, Rabiee SM (2012) Application of self-learning evolutionary algorithm for optimal design of a porous PMMA scaffold fabricated by laser drilling process. Published online, Process Mechanical Engineering
37. Moore M (1974) Symmetrical intersections of right circular cylinders. Math Gaz 58:181–185
38. Karageorgiou V, Kaplan D (2005) Review, Porosity of 3D biomaterial scaffolds and osteogenesis. Biomaterials 26:5474–5491
39. Hulbert SF, Young FA, Mathews RS, Klawitter JJ, Talbert CD, Stelling FH (1970) Potential of ceramic materials as permanently implantable skeletal prostheses. Biomed Mater Res 4:433–456
40. Nakayama Y, Matsuda T (1995) Surface microarchitectural design in biomedical applications: preparation of microporous polymer surfaces by an excimer laser ablation technique. J Biomed Mater Res 29(10):1295–301
41. Reimers H, Gold J, Kasemo B, Chakarov D (2003) Topographical and surface chemical characterization of nanosecond pulsed-laser micro-machining of titanium at 532 nm wavelength. Appl Phys A 77:491–8
42. Semak VV, Dahotre NB (1997) Laser surface texturing. In: Dahotre NB (ed) Lasers in surface engineering, surface engineering series: ASM International. Materials Park, OH, USA, pp 35–67
43. Mirhosseini N, Crouse PL, Schmidth MJJ, Li L, Garrod D (2007) Laser surface micro-texturing of Ti–6Al–4V substrates for improved cell integration. Appl Surf Sci 253:7738–7743 c
44. Nagahama H, Maeda H, Kashiki T, Jayakumar R, Furuike T, Tamura H (2009) Preparation and characterization of novel chitosan/gelatin membranes using chitosan hydrogel. Carbohydr Polym 76:255–260
45. Deligianni DD, Katsala ND, Koutsoukos PG, Missirlis YF (2001) Effect of surface roughness of hydroxyapatite on human bone marrow cell adhesion, proliferation, differentiation and detachment strength. Biomaterials 22(1):87–96